Progress In Electromagnetics Research, Vol. 125, 97–118, 2012

ULTRA WIDEBAND WAVE-BASED LINEAR INVERSION IN LOSSLESS LADDER NETWORKS

A. Shlivinski*

Department of Electrical and Computer Engineering, Ben-Gurion University of the Negev, Beer-Sheva 84105, Israel

Abstract—A wave-based inversion algorithm for the recovery of deviation in the values of elements of discrete lossless inductance-capacitance and capacitance-inductance ladder networks from their nominal values is formulated. The algorithm uses ultra wideband source excitation over the frequency range where forward and backward voltage and current waves propagate along the network. Employing a weak type scattering formulation renders the voltage wave reflection coefficient to be a $\mathcal{Z}$ transform of the sequence of perturbation in the value of the elements. Inversion of the reflected date from the transformed domain to the spatial domain by Fourier type integration yields the element's perturbations and consequently, the actual elements of the network. Demonstrations of the algorithm performance on several test cases show its efficacy as a non-destructive testing tool.

1. INTRODUCTION

Discrete types of periodic one-dimensional ladder networks are traditionally used in textbooks to study continuous transmission lines (TLs) [1, 2] or to model many physical phenomena. However, using appropriate chosen parameters, these types of structures, made either of lumped elements or of distributed elements that, to an extent, model lumped elements, can be realized to meet some prescribed properties. The renewed attention to applications of these types of networks as guided structures supporting the propagation of voltage and current waves is due to the progress in miniaturizing circuit elements and the possibility of assembling metamaterial TLs with desired properties (see, e.g., [3]). An additional issue of interest that apply to ladder

Received 8 January 2012, Accepted 13 February 2012, Scheduled 22 February 2012
* Corresponding author: Amir Shlivinski (amirshli@ee.bgu.ac.il).

structures as propagation media is the identification of, for example, faulty circuit elements that deviate from nominal values by applying non-destructive wave-based techniques. One such technique for these inherently discrete and therefore frequency dispersive structures is derived below within the framework of the weak scattering.

Although inversion in one-dimensional *continuous nonuniform* TLs to recover structural parameters [inductance (L), capacitance (C), resistance (R) and conductance (G)] was studied in the past (see, e.g., [4]), the subject has generated renewed interest in recent years [5, 6]. Inversion in discrete types of structures, where cascaded *continuos* TL sections of finite length are set consecutively is one aspect of discrete inversion (see in [7, 8]). Discrete inversion is also applicable to continuous medium that is spatially discretized or, alternatively, in which the spatial domain is set as a grid of lattice points. The inversion of *discretized* one-dimensional Schrödinger type equation can be found in, for example, [9], while the inversion of reflected waves in stratified elastic media for geophysics applications is given in [10]. A more recent inversion of a discrete Helmholtz equation for the recovery of the boundary impedance in a two-dimensional domain appears in [11]. An additional type of discrete inversion is for ladder-type networks, which are structures that are *a-priori spatially discrete*. A typical ladder network is assembled by series and parallel branches arranged in cascading order (Fig. 1). The elements on each of the branches can be either inductors, capacitors, resistors, or any combination of the three such to achieve wave propagation characteristics (see, e.g., [12, 13]). Inversion in an RC ladder-type structure has been studied to recover their parameters (see e.g., [14] which uses the layout of the poles and zero of the impedance) or to identify a single capacitance fault in RLC ladder networks [15]. Inversion in LC[†] type of ladder network where the capacitance elements are known and equal with a "peeling" type algorithm was carried out, recently, in [16].

In the present paper an inversion in "long" LC or CL lossless ladder networks is presented within a linearized framework for the recovery of the perturbations in the elements values relative to their nominal background values. To that end, the formulation uses ultra wideband excitation and decomposition of the nodal voltages into a combination of forward and backward propagating voltage waves. The inversion algorithm employes the exact Kirchhoff's current and voltage circuit relations to formulate an exact spatially discrete type of *homogeneous* Helmholtz equation in an *inhomogeneous* medium

[†] In an LC network, the series elements are inductors while the parallel elements are capacitors. In contrast, in CL networks, the series elements are capacitors while the parallel elements are inductors.

(network). Reformulation of the homogeneous Helmholtz equation as an *inhomogeneous* equation in a *homogeneous* background medium with induced driving sources yields a simple relation for the scattered waves in terms of the Green's function of the background medium. Though simple, the expression for the scattered waves is nonlinear in the unknown medium parameters. A linearized expression of the scattered voltage wave is obtained by using weak scattering conditions (small magnitude of the perturbations in the elements' values over those of the background medium). This linearization renders the reflection coefficient (back-scattered wave) as a filtered version of the $\mathcal{Z}$ transform of the sequence of perturbations that is evaluated at the frequency-dependent propagation constant. Exciting the network over a broad frequency range (the network's pass-band) leads to a tailing of the transformed domain (the "propagation constant" domain) with reflection-type data. Inversion of the data from the transformed domain to the spatial domain by a Fourier type integration yields the sequence of unknown perturbations. Thus implying that the formulation is of a direct inversion type (not iterative).

The paper is organized as follows. Problem formulation is outlined in Sec. 2, with the derivation of the corresponding Helmholtz equation in Sec. 2.1, and the wave propagation characteristics in the background medium are given in Sec. 2.2 (and in Appendix A) followed by the formulation of the scattered voltage wave within the weak scattering approximation. A discussion on the range of validity of the weak scattering approximation is given in Appendix B. The linear inversion is presented in Sec. 3 followed by a demonstration of the efficacy of the inversion algorithm for LC and CL types of ladder networks in Sec. 4. The discussion concludes with a summary in Sec. 5 with additional concluding remarks regarding the benefits in using the presented algorithm.

In the following discussion: V and I represent nodal voltage and branch currents, respectively, Z and Y represent series impedance and parallel admittance, respectively. The radian frequency is denoted by ω, with $e^{j\omega t}$ ($j = \sqrt{-1}$) the time dependence that is suppressed in the expressions below.

2. LAYOUT AND PROBLEM FORMULATION

Let's assume that the physical medium is of an electrical lossless network that is composed of N frequency dependent cascading "ZY_n", $n = 1, \ldots, N$ sections as depicted in Fig. 1 that are generally unknown. Each "ZY_n" section composed of a series impedance $Z_n(\omega) = z_n\zeta(\omega)$ and a parallel admittance $Y_n(\omega) = y_n\eta(\omega)$, where $\zeta(\omega)$ and $\eta(\omega)$

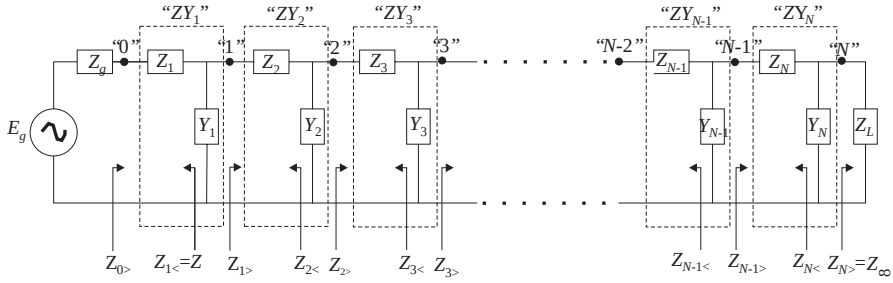

Figure 1. Layout of the ladder network.

are, generally, known frequency dependent functions and $\{z_n, y_n | \, n = 1, \ldots, N\}$ are generally unknown real parameters that correspond to the electrical values of the elements. The number of cascading sections N need not be known; moreover, it may also be that $N \to \infty$. It is assumed that each "ZY_n" constitutes an unknown deviation (perturbation) from a known *background* section "$\bar{Z}\bar{Y}$". A background section "$\bar{Z}\bar{Y}$" is composed of a series impedance $\bar{Z}(\omega) = \bar{z}\zeta(\omega)$ in conjunction with a shunt admittance $\bar{Y}(\omega) = \bar{y}\eta(\omega)$ ($\bar{z}$, $\bar{y}$ are known). Since the frequency dependence of $Z_n(\omega)$ and $\bar{Z}(\omega)$ is $\zeta(\omega)$ and that of $Y_n(\omega)$ and $\bar{Y}(\omega)$ is $\eta(\omega)$, the deviations are values of $\{z_n\}$ and $\{y_n\}$ from the background values $\bar{z}$ and $\bar{y}$, respectively[‡]. For the sake of simplicity, assume also that (*i*) the 1st and Nth sections "ZY_1'' = "ZY_N" = "$\bar{Z}\bar{Y}$", and (*ii*) the network is terminated on its lefthand side (node 0) by a voltage source $E_g(\omega)$ with input impedance $Z_g(\omega) = Z_\infty(\omega) - \bar{Z}(\omega)$ and on its right-hand side (node N) by a load $Z_L(\omega) = Z_\infty(\omega)$, where $Z_\infty(\omega)$ is the terminal impedance of such an infinite network composed of *background* "$\bar{Z}\bar{Y}$" sections. Note that in such a background network, Z_∞ is the solution of the following relation (see in Fig. 1) $Z_{n>} = \bar{Z} + (Z_{n+1>}^{-1} + \bar{Y})^{-1}$, upon noting that $Z_{n>} = Z_\infty$ for $n = 0, 1, \ldots, N$. These settings ensure matching of the network at its two terminals, furthermore, the background network appears as equivalent to a uniform infinite network nodes $1 \le n < N$. Additionally, the source's excitation frequency ω is constrained to the range $\omega \in \Omega = (\omega_{\min}, \omega_{\max})$, where Ω is the range of frequencies where the periodic unperturbed (background) network *supports propagation of voltage and current waves* (see the discussion in Sec. 2.2).

Following the formulation of the network's layout, the inverse

[‡] Note, for example, for a ladder network section composed of a series inductor and a shunt capacitor, $\zeta(\omega) = \eta(\omega) = j\omega$, while for a section that is composed of a series capacitor and a shunt inductor, $\zeta(\omega) = \eta(\omega) = 1/j\omega$. In both cases $\{z_n\}$ with z and $\{y_n\}$ with y are the inductance/capacitance and the capacitance/inductance, respectively.

problem is stated as follows: *For the ladder network as in Fig. 1 with* ***known*** *background sections "$\bar{Z}\bar{Y}$", find the set of perturbed unknown parameters $\{z_n, y_n | \, n = 2, \ldots, N-1\}$ and generally unknown N by using voltage measurements at terminal $n = 0$ carried out over a broad sweep of the source frequencies $\omega \in \Omega$.*

A wave-based solution to the inversion problems, as stated above, can be obtained by formulating the network's nodal voltages in terms of waves propagating along the network. This is carried out by using Kirchhoff's current and voltage laws [17] to give a *discrete Helmholtz equation* (the frequency domain counterpart of the discrete wave equation) that governs forward and backward wave propagation. Since a wave-based solution is sought, it is convenient to refer to each perturbed section as a "scatterer" and the perturbation in the voltages along the network over the quiescent, background voltages as "scattered voltage". This paradigm is adopted in the following discussion of the problem's mathematical formulation.

In the rest of the paper, explicit indication of ω is omitted from all the frequency-dependent parameters.

2.1. Circuit Relations and the Helmholtz Equation

The mathematical formulation of the problem begins with the circuit's Kirchhoff laws [17]. To this end, a current I_n is defined as flowing through the Z'_nth element in the direction of node n, and a voltage V_n is defined as the voltage across the Y'_nth element (see Fig. 2). Consequently, the following two iterative equations can be formulated:

$$V_{n-1} = I_n Z_n + V_n, \quad I_n = V_n Y_n + I_{n+1}. \tag{1}$$

Representing I_n and I_{n+1} in terms of the three nodal voltages V_{n-1}, V_n, and V_{n+1}, gives rise to the following *discrete Helmholtz equation* of the ladder network:

$$\frac{V_{n+1}}{Z_{n+1}} - \left[\frac{1}{Z_{n+1}} + \frac{1}{Z_n} + Y_n\right] V_n + \frac{V_{n-1}}{Z_n} = 0, \quad n = 1, \ldots, N-1, \tag{2}$$

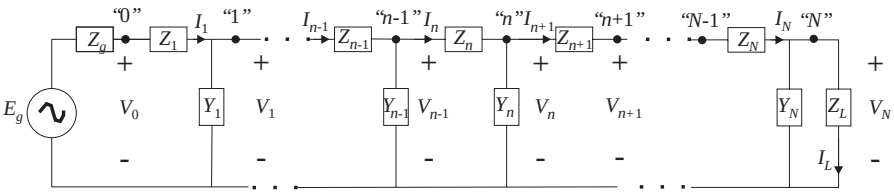

Figure 2. Network layout with the currents and voltages notations at the Network's terminals.

with additional boundary conditions at the source and load terminals. Equation (2) governs the propagation of voltage waves on a general ladder network. Note that Equation (2) can be rearranged in the form of a second-order Sturm-Liouville difference equation [18], whence it may be recognized as the discrete analog of a Helmholtz equation in a continuous inhomogeneous medium when both the permittivity and permeability can vary in space [19].

Equation (2) is a homogeneous equation in an inhomogeneous medium. Rearranging it as an inhomogeneous equation in a homogeneous medium with additional induced sources simplifies its use for the inversion problem. To that end, $1/\bar{Z}$ is added to and subtracted from each inverse impedance term in Equation (2), and similarly, $\bar{Y}$ is added to and subtracted from each admittance term followed by multiplication by $\bar{Z}$ and rearrangement, to give

$$V_{n+1}-[2+\xi]V_n+V_{n-1}=\bar{\delta}_{z_{n+1}}V_{n+1}-\left[\bar{\delta}_{z_{n+1}}+\bar{\delta}_{z_n}+\xi\bar{\delta}_{y_n}\right]V_n+\bar{\delta}_{z_n}V_{n-1}. \quad (3a)$$

where $\xi = \bar{Z}\bar{Y} = \bar{z}\bar{y}\eta(\omega)\zeta(\omega)$, and the relative perturbations are defined by

$$\bar{\delta}_{z_n} = 1 - \frac{\bar{Z}}{Z_n} = 1 - \frac{\bar{z}}{z_n}, \quad \bar{\delta}_{y_n} = 1 - \frac{Y_n}{\bar{Y}} = 1 - \frac{y_n}{\bar{y}}. \quad (3b)$$

For simplicity, let us also define the series $\{\bar{\delta}_p\}$, which is composed by interlacing values of $\bar{\delta}_{z_n}$ and $\bar{\delta}_{y_n}$, such that

$$\bar{\delta}_{2p-1} = \bar{\delta}_{z_p}, \quad \bar{\delta}_{2p} = \bar{\delta}_{y_p}. \quad (3c)$$

Thus giving the source term on the righthand side of Equation (3a) to be read as

$$S(\bar{\delta}_n, V_n) = \bar{\delta}_{2n+1}V_{n+1} - \left[\bar{\delta}_{2n+1} + \bar{\delta}_{2n-1} + \xi\bar{\delta}_{2n}\right] V_n + \bar{\delta}_{2n-1}V_{n-1}. \quad (3d)$$

The lefthand side of Equation (3a) is a difference form that corresponds to that of a homogeneous background ladder network ("$\bar{Z}\bar{Y}$" sections), whereas the actual inhomogeneity is represented by the induced (voltage-dependent) sources on the righthand side. These sources result due to the scatterers contrast (perturbation in the circuit elements) with the background.

A scattered wave formulation is obtained by the the following decomposition:

$$V_n = V_n^i + V_n^s \quad (4)$$

where V_n^i is the *incident* voltage wave propagating in the unperturbed background and homogeneous network while V_n^s is the *scattered* voltage propagating in the network due to the inhomogeneity, $\{z_n, y_n | \, n = 2, \ldots, N-1\}$, of the actual network. By its definition, the incident voltage satisfies the homogeneous Helmholtz equation in the

unperturbed background network, (compare Equation (3a)): $V^i_{n+1} - [2+\xi]\,V^i_n + V^i_{n-1} = 0$ with the boundary condition $V^i_0 = E_g\,Z_{0>}[Z_{0>} + Zg]^{-1}$, where $Z_{0>} = Z_\infty$, thus rendering Equation (3a)

$$V^s_{n+1} - [2+\xi]\,V^s_n + V^s_{n-1} = S(\bar{\delta}_n, V_n), \tag{5}$$

It is noted that Equation (5) is arranged such that the difference form on the left is associated with the discrete Helmholtz equation of the unperturbed background network while the induced sources due to the perturbations are grouped to the right. The solution for the scattered voltage V^s_n can now be presented in terms of the characteristic properties of the background network. To that end, the characteristics of voltage wave propagation on such a background network is discussed next, followed by a solution of Equation (5) in Sec. 2.3.

2.2. Wave Propagation in the Background Network

Voltage wave propagation along a terminally matched background medium (network) characterized by "$\bar{Z}\bar{Y}$" sections is summarized here in terms of wave propagation along infinite networks (for additional discussion the reader is referred to Appendix A). The applicability of infinite network condition is possible since the matching boundary conditions at the network terminals $Z_{1<} = Z_{N>} = Z_\infty$ render the behavior of any voltage wave-mode propagation as if it were propagating along an infinite network. Voltage wave propagation along an infinite network is characterized by the two eigen-solution of the second order homogeneous difference Helmholtz equation (see, e.g., the lefthand side of Equation (5)):

$$V^{(1)}_n = \alpha^n, \quad V^{(2)}_n = \alpha^{-n} \tag{6a}$$

where α is the discrete "propagation constant" that is given by

$$\alpha = e^{j\phi} = \begin{cases} \alpha_1, & \text{if } \phi'_1 > 0, \\ \alpha_2, & \text{if } \phi'_2 > 0. \end{cases} \tag{6b}$$

with

$$\alpha_{1,2} = \frac{1}{2}\left[(2+\xi) \pm j\sqrt{4-(2+\xi)^2}\right], \tag{6c}$$

or alternatively by $\alpha_{1,2} = e^{j\phi_{1,2}}$, where $\tan\phi_{1,2} = \pm\sqrt{4-(2+\xi)^2}/(2+\xi)$, the indexes $1, 2$ correspond to the upper and lower $\pm$ signs, respectively. The choice between $\alpha_{1,2}$ in (6b) ensures that the energy flow is directed from the source (at terminal "0") to the actual network, see the additional discussion in Appendix A.

Wave propagation along the network occurs whenever a progressive phase is accumulated as the index n monotonically changes

(n is the spatial index). Thus, it requires $\mathrm{Im}\{\alpha_{1,2}\} \neq 0$, which leads to $4-(2+\xi(\omega))^2 > 0$, giving the system of inequalities:

$$-4 < \xi(\omega) < 0. \tag{7}$$

Solving Equation (7) for ω gives the range of excitation frequencies, the *pass-band*, $\Omega = (\omega_{\min}, \omega_{\max})$, where waves can propagate along the discrete structure, with $\omega_{\min}$ and $\omega_{\max}$ the lower and upper cut-off frequencies, respectively. An $\omega \in \Omega$ implies by Equation (6c) that $|\alpha_{1,2}| = 1$, and $\alpha_1 = \alpha_2^* = 1/\alpha_2$ ($*$ denotes complex conjugation).

Having defined the two wave-modes in (6) and the frequency pass-band via(7) it can be noted that $V_n^{(1)}$ is a voltage wave propagation in the backward (left, "negative") direction that satisfies the boundary conditions at $n \to -\infty$ and $V_n^{(2)}$ is a voltage wave propagating in the forward (right, "positive") direction that satisfies the boundary condition at $n \to \infty$. Consequently, the background medium Green's function is given by (see in [18, Theorem 2.3.8, 20]),

$$G_{n,m} = -\frac{\alpha^{-|n-m|}}{\alpha - \alpha^{-1}}. \tag{8}$$

Finally, with α given by Equation (6b), it follows that $Z_\infty = (\alpha - 1)\bar{Y}^{-1}$ where it is the solution of $Z_{n>} = \bar{Z} + (Z_{n+1>}^{-1} + \bar{Y})^{-1}$ with $Z_{n>} = Z_\infty$ for $n = 0, 1, \ldots, N$ in the background network [12, 13].

2.3. The Scattered Voltage Wave

The scattered voltage wave can now be obtained from Equation (5) using discrete convolution with the Green's function of the background medium Equation (8) to yield

$$V_n^s = \sum_m G_{n,m} S(\bar{\delta}_m, V_m), \tag{9}$$

with $m = 1, 2, \ldots, N$. Note that Equation (9) is nonlinear in the perturbation sequence $\{\bar{\delta}_m\}$ since it appears explicitly in S and implicitly via $V_n = V_n^i + V_n^s$, which also depend on it. In the following discussion, a linearized solution to Equation (9) is sought within the *weak scattering approximation* (Born type approximation [21]).

The weak scattering linearization of Equation (9) makes use of the following assumption: since the perturbations $\{\bar{\delta}_{z_n}, \bar{\delta}_{y_n}\}$ are small ("weak") compared to z and y, the scattered voltage V_n^s is also a small perturbation, to first order, in V_n^i ($|V_n^s| \ll |V_n^i|$), indicated by $\bar{\delta}_{V_n}$. Inserting the decomposition of Equation (4) into Equation (9), noting via Equation (3d) that $S(\bar{\delta}_m, V_m) = S(\bar{\delta}_m, V_m^i) + S(\bar{\delta}_m, \bar{\delta}_{V_m})$

and retaining explicitly only first order perturbation terms, then the scattered wave becomes:

$$V_n^s = \sum_m G_{n,m} S(\bar{\delta}_m, V_m^i) + \mathcal{O}(\bar{\delta}^2) \tag{10}$$

where the source term $S(\bar{\delta}_m, V_m^i)$ is linear in $\{\bar{\delta}_m\}$, and $\mathcal{O}(\bar{\delta}^2) \sim S(\bar{\delta}_m, \bar{\delta}_{V_m})$ represents the higher order terms of at least second order in the perturbations. For further treatment of Equation (10), the weak nonlinear $\mathcal{O}(\bar{\delta}^2)$ term is neglected, thus rendering the equation linear in $\{\bar{\delta}_m\}$. A discussion on the range of validity of the weak scattering solution is given in Appendix B. Note that an exact representation of the higher order terms that extends the range of validity of such weak scattering approximations can be obtained by expanding V_n^s into a series of higher order perturbed contributions within the perturbation theory framework as was carried out for continuous media in [22–24] or, alternatively, as in [25].

The nodal voltage measured at node "0" records the backward propagating component of the scattered wave due to the excitation at node "0". Recalling the discussion in Sec. 2.2 that $V_n^i = V_0^i \alpha^{-n}$ is the voltage wave propagating in the background network in seemingly infinite network conditions ("matched" where $Z_{n>} = Z_{n+1>} = Z_N = Z_\infty$) with $V_0^i = Z_\infty \left[Z_g + Z_\infty\right]^{-1} E_g$. Inserting V_n^i into Equation (9) and noting that $m > 0$, the measured component of the scattered wave is given by

$$V_0^s = V_0^i \frac{\alpha - 1}{\alpha + 1} \left\{ \sum_m \alpha^{-2m} \bar{\delta}_{2m} + \sum_m \alpha^{-(2m+1)} \bar{\delta}_{2m+1} \right\} = V_0^i \Gamma_0 \tag{11a}$$

$$\Gamma_0 = \frac{\alpha - 1}{\alpha + 1} \tilde{\delta}(\alpha), \tag{11b}$$

where $\Gamma = V_0^s / V_0^i$ is voltage reflection coefficient, and $\tilde{\delta}(\alpha)$ was obtained by combining the two summations in Equation (11a) into one summation to give

$$\tilde{\delta}(\alpha) = \sum_p \alpha^{-p} \bar{\delta}_p, \quad p = 0, 1, \ldots, \quad \bar{\delta}_0 = 0. \tag{11c}$$

It is readily noted that $\tilde{\delta}(\alpha)$ is the $\mathcal{Z}$ transform (see in [26] of the sequence $\bar{\delta}$ evaluated on the complex point $\alpha(\omega)$. As we have seen above, in the propagation regime [see, e.g., Equation (7)], where $\alpha = e^{j\phi}$ with $\phi \in (0, \pi)$, it follows that $\tilde{\delta}(\alpha)$ may also be recognized as the discrete-index-continuous-spectral-parameter Fourier transform (known also as discrete time Fourier transform, DTFT [26]).

Equation (11b) establishes that within the weak scattering approximation, the reflection coefficient is obtained as a mapping ($\mathcal{Z}$-transform) between the discrete domain of sequences to the domain of frequency dependent propagation constants (the "spectral domain"). Moreover, in the transformed complex domain ("α" domain), the reflection coefficient is mapped into a circular arc of radius $|\alpha|$ about the origin and angle $|\phi(\omega_{\max}) - \phi(\omega_{\min})|$.

Having formulated the model for the scattered voltage wave V_0^s or, correspondingly, the reflection coefficient Γ_0 as in Equation (11), the next step is the introduction of the inversion algorithm for the recovery of $\bar{\delta}$ in Sec. 3.

3. LINEAR INVERSION

Performing broad frequency ranged voltage measurement at terminal "0" for $\omega \in \Omega$ gives V_0, from which the scattered voltage wave V_0^s can be obtained and the reflection coefficient $\Gamma_0 = (V_0/V_0^i) - 1 = V_0^s/V_0^i$. Assuming weak scattering conditions, Equation (11b) provides a linear model for the reflection coefficients as a function of the network's parameters in terms of a $\mathcal{Z}$ transform mapping (or the DTFT) of the interlaced perturbation series. Thus, inverting $\tilde{\bar{\delta}}(\alpha)$ with $\alpha = \alpha(\xi(\omega))$ from the "spectral (propagation constant) domain" to the index domain recovers the perturbation series $\{\bar{\delta}_n\}$ and $\{z_n, y_n\}$. To this end, following Equation (11b), denotes

$$G = \frac{\alpha+1}{\alpha-1}\Gamma_0 = -j\cot\left(\frac{\phi}{2}\right)\Gamma_0 \stackrel{\circ}{=} \tilde{\delta}(\alpha), \tag{12a}$$

where $\stackrel{\circ}{=}$ indicates equality of the measured quantity (Γ_0) with the model ($\tilde{\delta}$) subject to the model assumptions and the range of validity of the parameters as discussed in Sec. 2. Note that, Equation (12a) suggests that G is a filtered version of the actual reflection coefficient. The measured data is known over the frequency span Ω that corresponds to $\xi \in (-4, 0)$, and consequently, $\phi \in (0, \pi)$. Define an integration kernel $J(\omega)e^{jm\phi}$, with $m = 1, 2, \ldots$ and $J(\omega) = \phi' = \partial\phi/\partial\omega$ (see the discussion on ϕ' in Sec. 2.2) is a continuos function. Multiply Equation (12a) by the integration kernel and perform integration over the whole frequency band Ω,

$$\int_{\omega_{\min}}^{\omega_{\max}} d\omega\, G(\omega)J(\omega)e^{jm\phi} \stackrel{\circ}{=} \int_{\omega_{\min}}^{\omega_{\max}} d\omega\, \tilde{\delta}(\omega)J(\omega)e^{jm\phi(\omega)}. \tag{12b}$$

Next, focusing on the righthand side of the integration and changing the integration variable from ω to ϕ, we note that (i) $d\phi = d\omega\,\phi'$; (ii) for Ω that occupies whole of the available wave propagation frequency

band, the range of ϕ is given by $\phi(\omega_{\min}) \to 0$ and $\phi(\omega_{\max}) \to \pi$ or $\phi(\omega_{\min}) \to \pi$ and $\phi(\omega_{\max}) \to 0$

$$\int_{\omega_{\min}}^{\omega_{\max}} d\omega \tilde{\delta}(\omega) J(\omega) e^{jm\phi(\omega)} = \int_{\omega_{\min}}^{\omega_{\max}} d\omega \phi'(\omega) \tilde{\delta}(\omega) e^{jm\phi(\omega)} = \int_0^{\pi} d\phi \ \tilde{\delta}(\phi) e^{jm\phi}. \tag{12c}$$

It is readily noted that in view of the inverse DTFT [26], the rightmost integration is recognized as the analytic continuation of the series $\bar{\delta}_m$

$$\frac{1}{\pi} \int_0^{\pi} d\phi \ \tilde{\delta}(\phi) e^{jm\phi} = \bar{\delta}_m + j h_m \circledast \bar{\delta}_m \tag{12d}$$

where $\circledast$ is the discrete convolution operation and

$$h_m = \begin{cases} 0, & m \text{ even} \\ \frac{2}{m\pi}, & m \text{ odd.} \end{cases} \tag{12e}$$

is the discrete Hilbert transform kernel [26]. Recalling that $\{\bar{\delta}_m\}$ is a real sequence, the real part of the integral indeed yields the unknown perturbation sequence. Finally, combining Equation (12b) with Equation (12d) yields the inversion formula for obtaining the unknown perturbations

$$\bar{\delta}_m \stackrel{\circ}{=} \frac{1}{\pi} \mathrm{Re} \int_{\omega_{\min}}^{\omega_{\max}} d\omega \, G(\omega) \phi'(\omega) e^{jm\phi}, \quad m = 1, 2, \ldots. \tag{13}$$

Equation (13) is the final inversion expression. To this end, it relates the filtered version of the measured reflected data G [see the discussion at the beginning of this section and Equation (12a)] with the perturbation series $\{\bar{\delta}_m\}$ (or its recovered version) by a Fourier type integration.

It should be noted once G was calculated, $\bar{\delta}_m$ can readily be calculated by performing the integration in Equation (13) for any value of m. Inserting the recovered $\{\bar{\delta}_m\}$ into Equation (3c) with Equation (3b) yields the actual perturbations $\{\bar{\delta}_{z_m}, \bar{\delta}_{y_m}\}$ in the elements values. Finally, It can be argued that subject to the weak scattering assumption, $\bar{\delta}_m$ is recovered as zero whenever the corresponding z_n or y_n equals the background parameters $\bar{z}$ and $\bar{y}$, respectively, which can lead to termination of the algorithm at high enough m and the identification of N. These observations conclude the inversion formulation.

4. EXAMPLE

This section presents several examples of the use of the imaging algorithm of Equation (13) for different types of ladder networks and

different perturbations in the lumped element values (i.e., different scatterers) over the nominal background network.

In the examples below, the background network is composed of inductors and capacitors in different arrangements (LC or CL type of sections), with inductance $\bar{L} = 4/5H$ and capacitance $\bar{C} = 3/8F$. The excitation voltage source is assumed to be constant $E_g = 1$ for all $\omega \in \Omega$. The reflection data that is used as an input to the imaging algorithm, i.e., scattered voltage V_0^s or reflection coefficient Γ_0, is generated synthetically by the following procedure:

(i) Assume there is given a set of actual inductors and capacitors $\{L_n, C_n | \, 2 \leq n \leq N-1\}$ such that some or all of its elements differ (perturbed) from the nominal background elements $\bar{L}$ and $\bar{C}$.

(ii) The input impedance, Z_{in} (at node "0"), is given by the iterative calculation (see Fig. 1), $Z_{n>} = Z_n + \left[Z_{n+1>}^{-1} + Y_n\right]^{-1}$, with $Z_N = Z_\infty$, $n = N-1, N-2, \ldots, 0$ and $Z_{in} = Z_{0>}$, where the propagation constant α was set according to the discussion in Sec. 2.2.

(iii) The actual, perturbed node "0" voltage, V_0 is given by $V_0 = E_g Z_{in} / [Z_g + Z_{in}]$.

(iv) Recognizing that $V_0 = V_0^i [1 + \Gamma_0]$ where $V_0^i = E_g Z_\infty / [Z_g + Z_\infty]$ is the forward propagating (incident) voltage in the background network yields

$$\Gamma_0 = \frac{Z_{in}}{Z_\infty} \frac{Z_\infty + Z_g}{Z_{in} + Z_g} - 1. \tag{14}$$

This reflection coefficient is the input for the inversion algorithm of Equation (13) with $G(\omega)$ given in Equation (12a) and ϕ' as given in Sec. 2.2.

4.1. Inversion in an *LC* Network

In this section we consider an LC type of network assembled by sections, each comprising a series inductor followed by a parallel capacitor. For these types of elements, $\zeta(\omega) = \eta(\omega) = j\omega$ giving $\xi = -\omega^2 \bar{L}\bar{C}$. Following Equation (7), the frequency range $\Omega = (\omega_{\min}, \omega_{\max})$ with $\omega_{\min} = 0$ and $\omega_{\max} = 2/\sqrt{\bar{L}\bar{C}} = 3.6515\,\text{rad/sec}$, which suggests that this is a low-pass type of network.

For the first example, consider the following weak perturbation sequences in the elements $\{L_n\} = \bar{L} + 0.001\bar{L} \times [0\,0\,0\,2\,2\,(-2)\,(-2)\,0\,0\,0\,0\,0]$ and $\{C_n\} = \bar{C} + 0.001\bar{C} \times [0\,1\,1\,1\,1\,0\,0\,0\,0\,0\,1\,(-1)]$ that are embedded within the background network. In view of Equation (3b) and recalling that $z_n = \zeta(\omega) L_n$ and $y_n = \eta(\omega) C_n$, these perturbations give $\bar{\delta}_{z_n} = 1 - \bar{L}/L_n$ and $\bar{\delta}_{y_n} = 1 - C_n/\bar{C}$ and the corresponding profile of the

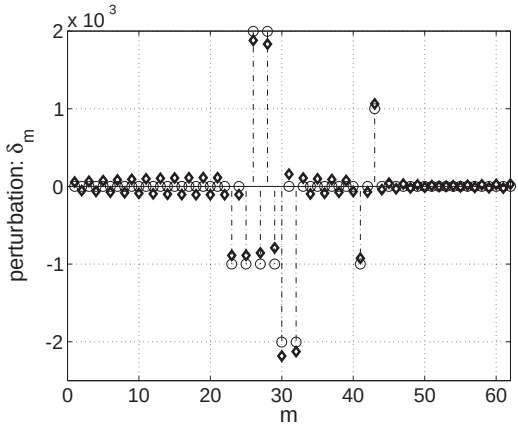

Figure 3. The first example of an LC network. The actual and reconstructed perturbation profiles $\{\bar{\delta}_n\}$ are represented by the ◯ and ◊ symbols, respectively, at the tips of the dashed-dotted lines.

interlaced sequence $\{\bar{\delta}_n\}$ [see Equation (3)], which is marked in Fig. 3 by the '◯' symbols at the tips of the dashed-dotted lines. These perturbation parameters were used in conjunction with the above background parameters to generate the reflection data Γ_0 as in items i–iv in the procedure above. The reflection coefficient Γ_0, was then, used as the input to the inversion algorithm of Sec. 3 to yield the "reconstructed perturbation" $\{\bar{\delta}_n\}$ of Equation (13) with $G(\omega)$ of Equation (12a) and ϕ' of Sec. 2.2. The integration in Equation (13) was calculated by numerical quadrature employing the entire available frequency span Ω. The reconstructed perturbation sequence $\{\bar{\delta}_n\}$ is depicted in Fig. 3 by the ◊ shaped symbols. It can be noted by comparing the reconstructed perturbations to the actual perturbations (◊ and ◯ symbols, respectively) that the imaging algorithm indeed recovered the relative location of the perturbations, and a near exact recovery of the magnitude of the perturbation was also achieved. The small error emerges in the reconstruction comes since the sum of the perturbation sequence deviates from zero, therefore introducing an error, see the discussion in Appendix B.

It should be noted that the number of sections of the network N has no role in the reconstruction algorithm. This is because attempting to reconstruct perturbations with indexes greater than approximately $2N$ (two elements per section), which here is about 43 yields $\bar{\delta}_m \approx 0$, for $m > 43$. This is as expected since the network is loaded with $Z_N = Z_\infty$ that effectively models background network with identically zero perturbation.

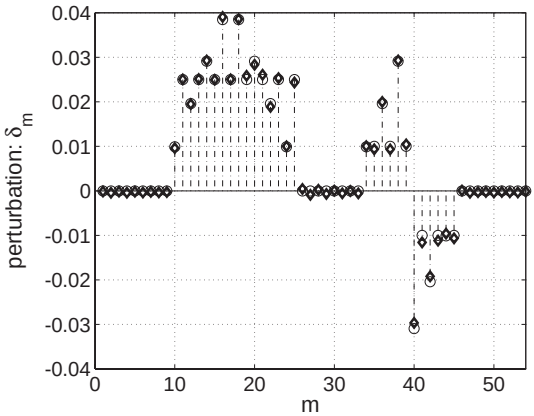

Figure 4. Same as in Fig. 3 but for the second example.

For the second example, the following perturbation parameters were set: $\{L_n\} = \bar{L} + 0.01\bar{L} \times [1\,2\,3\,4\,4\,3\,2\,1\,0\,0\,0\,0\,1\,2\,3\,(-3)\,(-2)\,(-1)]$ and $\{C_n\} = \bar{C} + 0.01\bar{C} \times [(-2.5)\ (-2.5)\ (-2.5)\ (-2.5)\ (-2.5)\ (-2.5)(-2.5)\ (-2.5)\ 0\ 0\ 0\ 0\ (-1)\ (-1)\ (-1)\ 1\ 1\ 1]$, see the '◯' symbols at the tips of the dashed-dotted lines in Fig. 4 that correspond to $\{\bar{\delta}_n\}$. As in the first example, the simulated Γ_0 of Items i–iv above is used as the input for the inversion of Equation (13). The reconstructed perturbation sequence $\{\bar{\delta}_n\}$ is depicted in Fig. 4 by the ◊ shaped symbols. It can be readily noted that the reconstructed profile is in excellent agreement with the actual perturbation sequence in both its relative location along the network and amplitude (compare the ◊ and ◯ symbols, respectively).

The results of the second example in Fig. 4 seem somewhat better than those of the first example in Fig. 3, even though the perturbation magnitudes here are approximately 10 times those used in the first example in Fig. 3. In fact, it can be shown that in both examples the sum $|\sum_m \bar{\delta}_{z_m} - \sum_m \bar{\delta}_{y_m}|$ is of the same order of magnitude. However, relative to the average perturbation magnitude in the second example, this sum is lower, therefore denoting the improvement in the reconstruction. It should be noted that for LC type networks with the definition of $\bar{\delta}_{z_n}$ in Equation (3b), though the sum of the perturbation sequence $\{\bar{L} - L_n\} \to 0$, the corresponding sum of $\bar{\delta}_{z_n} \nrightarrow 0$.

The last example in this section comprises 30 perturbed sections that are constructed from 1) series inductors with a normal distribution with mean $\bar{L}$ and standard deviation $0.005\bar{L}$, i.e., $L_n \sim \mathcal{N}(\bar{L}, 0.005\bar{L})$; and 2) parallel capacitors that also have a mean $\bar{C}$ and standard deviation $0.005C_n$, i.e., $C_n \sim \mathcal{N}(\bar{C}, 0.005\bar{C})$. As in the previous two

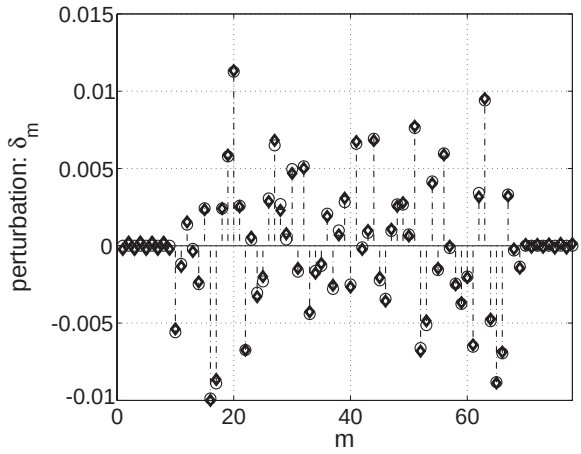

Figure 5. Same as in Fig. 3 but for the third example.

examples, Fig. 5 depicts the actual and reconstructed perturbations, which are represented by ◯ and ◊ symbols, respectively. A very good agreement is obtained between the actual and the reconstructed profiles. The negligible discrepancy between the two profiles stems mainly from the fact that although the perturbations are normally distributed with zero mean, the actual perturbation sequences are finite in length, and therefore, their actual sum (or mean) deviates from zero (see the discussion in Appendix B).

4.2. Inversion in a *CL* Network

In this section we consider a CL type of network assembled by sections, each of which comprises a series capacitor followed by a parallel inductor. This type of network facilitates a "lefthand" type of discrete transmission line [3]. For this type of section $\zeta(\omega) = \eta(\omega) = (j\omega)^{-1}$, giving $\xi = -(\omega^2 \bar{L}\bar{C})^{-1}$. Using Equation (7), it follows that this is a high-pass type of network with a lower cut-off frequency $\omega_{\min} = 1/\sqrt{4\bar{L}\bar{C}} = 0.9129\,\text{rad/sec}$ and $\omega_{\max} \to \infty$. The actual network consists of 20 sections that were randomly perturbed as in the third example in Sec. 4.1 with parallel inductors $L_n \sim \mathcal{N}(\bar{L}, 0.005\bar{L})$ and series capacitors $C_n \sim \mathcal{N}(\bar{C}, 0.005\bar{C})$. The reconstructed profile, following Equation (13) (with $G(\omega)$ of Equation (12a) and ϕ' of Sec. 2.2), and the actual profile, are depicted in Fig. 6 with the ◊ and ◯ symbols, respectively. As in the previous examples, here too, a good agreement is obtained between the actual and the reconstructed profiles.

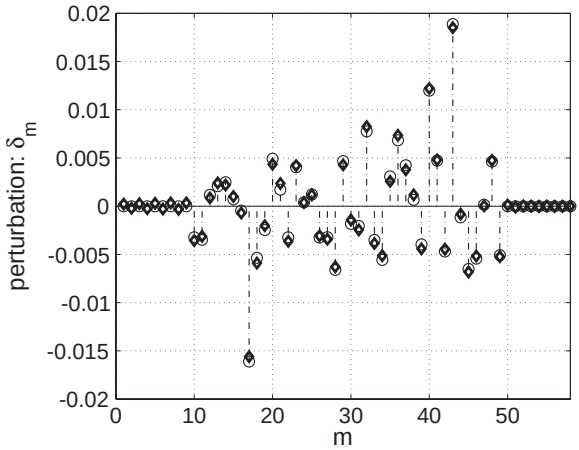

Figure 6. An example of a CL network. The actual and reconstructed perturbation profiles $\{\bar{\delta}_n\}$ are represented by the ◯ and ◊ symbols, respectively, at the tips of the dashed-dotted lines.

5. SUMMARY AND CONCLUSIONS

A linearized wave-based inversion algorithm for the recovery of lossless inductance and/or capacitance type scattering elements (scatterers) embedded within a lossless ladder network was presented. The algorithm assumes that the scatterers are modeled by a weak perturbation sequence over the known background medium (network). Assuming also that the network actually models a discrete guided wave structure (a transmission line), the nodal voltage and branch currents are decomposed by voltage/current waves traveling along the network. Formulating Kirchhoff's equations and the associated discrete Helmholtz equation followed by the weak scatterer assumptions renders the nonlinear equation for the perturbed elements linear, though frequency dispersive, see in Sec. 2.3. The range of validity of the weak scatterer assumption giving the linear inversion was discussed Appendix B. Within the weak scattering assumption, it was shown that the backscattered wave voltage (reflection coefficient) is linearly proportional to the $\mathcal{Z}$ transform (or a discrete Fourier transform) of the perturbation sequence evaluated at the complex frequency-dependent discrete "propagation constant", Equation (11b). Using scattered data, of back-reflection type, recorded over a broad sweep of frequencies where wave propagation takes place allows for the inversion of the transformed perturbation sequence by a Fourier type integration giving the actual profile of the transmission line in Equation (13). The algorithm was demonstrated in Sec. 4 through

several examples of righthanded LC and lefthanded CL discrete transmission lines. The examples demonstrates the efficacy of the algorithm in recovering random distribution of weak perturbation in the network L and C elements over nominal background elements.

To conclude the discussion, the newly introduced algorithm presented here is of a one-dimensional discrete filtered backpropagation type [recall that a continuos version of a filtered backpropagation algorithm is used for diffraction tomography in *spatially continuous structures* within the Born and Rytov approximations (see, e.g., [21, 27]]. It should also be pointed that the benefits in using this algorithm for recovering weak perturbations are: (i) the formulation makes use of the fact that the network is, by its definition, spatially discrete and *not discretized* and assembled of lumped elements (unlike [7, 8]) and consequently there is an associate inherent frequency dispersion that is accommodated in the inversion; (ii) it renders the inversion, simply, of a direct inverse Fourier transform type without any iterative procedure as in other techniques (see e.g., [7, 8, 10, 14, 16]), and without any need for an a-priori knowledge of the size of the network (number of ZY sections); (iii) it recovers the perturbations in both the parallel and series elements (inductance and capacitance and vice versa) over a known background (unlike [15, 16]) and for all sections of the network; and (iv) the proposed algorithm can be used for both LC and CL networks without any differences. Recalling that CL networks as propagation environments are interesting in connection with metamaterials where the presented algorithms is among the first to suggests imaging in such structures/networks.

Finally, and on a broader perspective, the study of wave propagation and its application in physically pre-defined, inherently discrete structures (and not discretized continuous structure) is gaining importance since these types of structures/networks offer a wide range of — e.g., synthesizing new materials — within the metamaterial framework. To that end, here we discuss one such wave-based application in the field of non-destructive testing of discrete structures.

APPENDIX A. DISCRETE PROPAGATION CONSTANT AND ENERGY FLOW

This appendix provides further details on the characteristic properties of the "discrete propagation" constant α that are used to set (6). To that end, assume, first, that a wave-mode solution of the second order homogeneous difference Helmholtz equation $V_{n+1}-(2+\xi)V_n+V_{n-1}=0$ is given by $V_n = 1/\alpha^n$, see in [12]. It follows that α is a root of the characteristic polynomial (dispersion relation) [20] $\alpha^2-(2+\xi)\alpha+1=0$

giving the two possible solutions for α in (6c). Noting in Equation (6c) that since $\xi = \xi(\omega) = \bar{z}\bar{y}\zeta(\omega)\eta(\omega)$, it renders $\alpha_{1,2} = \alpha_{1,2}(\omega)$; furthermore $\alpha_1 \cdot \alpha_2 = 1$

Upon defining the discrete propagation constant in (6) and the frequency *pass-band*, $\Omega = (\omega_{\min}, \omega_{max})$, in Equation (7) it follows that: (i) $\omega \in \Omega$ implies by Equation (6c) that $|\alpha_{1,2}| = 1$, and $\alpha_1 = \alpha_2^* = 1/\alpha_2$ ($*$ denotes complex conjugation). Denoting $\alpha_{1,2} = e^{j\phi_{1,2}}$, where $\tan\phi_{1,2} = \pm\sqrt{4-(2+\xi)^2}/(2+\xi)$ gives $\phi \in (0,\pi)$ for $\omega \in \Omega$ with $\phi \to 0, \pi$ as $\xi \to 0, -4$, respectively. (ii) for $\omega \notin \Omega$, i.e., *stop-band*, $\alpha_{1,2} = \frac{1}{2}[(2+\xi) \pm \sqrt{(2+\xi)^2-4}] \lesseqgtr 1$ is a real number, resulting in pure decay or growth in the waves amplitude along the network. Note that in a lossy network, there could be decaying wave propagation conditions since α is a complex number.

As was discussed in Equation (6), in the propagation scenario ($\omega \in \Omega$) the aim is the delivery of energy from the source (at terminal "0") by forward propagating waves and the reception of scattered energy (at terminal "0") by backward propagating waves. To each of these wave modes, $\alpha_{1,2}$ is assigned in light of the sign (direction) of the group velocity (delay) v_g, which corresponds to the energy wave speed and the $e^{j\omega t}$ time dependence. It can be shown that $v_{g_{1,2}} \sim (\phi'_{1,2})^{-1}$, where $\phi'_{1,2} = \partial\phi_{1,2}/\partial\omega = \mp\xi'[4-(2+\xi)^2]^{-1/2}$ with $\xi' = \partial\xi/\partial\omega$. It follows that for an LC type network, where $\xi = -\omega^2 LC$ (see the discussion in Sec. 4.1), α_1 denotes $v_{g_1} > 0$ and α_2 denotes $v_{g_2} < 0$. On the other hand, for a CL type network, where $\xi = -(\omega^2 LC)^{-1}$ (see the discussion in Sec. 4.2), α_1 denotes $v_{g_1} < 0$ and α_2 denotes $v_{g_2} > 0$. These guidelines lead to the choice of α in Equation (6).

APPENDIX B. RANGE OF VALIDITY OF THE LINEARIZATION

The weak scattering approximation made in Sec. 2.3 leading to the linearized solution in Equation (10) or Equation (11) is valid for a certain range of values of the perturbations $\{\bar{\delta}_{z_n}, \bar{\delta}_{y_n} | 2 \le n \le N-1\}$. In that context, two constraints need to be met to validate the approximation:

(i) **Reflection type constraint:** The scattered wave field at node n can be decomposed into two scattered components: (i) backscattered voltage wave contribution due to scattering from sections $\{ZY_m\}$ with $n < m \le N-1$; and (ii) forward scattered voltage wave due to scattering from sections $\{ZY_m\}$ with $2 < m < n$. In either case the combined contribution of the scattered components giving V_n^s should be weak in comparison to the

excitation wave, i.e., $|V_n^s| \ll |V_n^i|$. A simple and general expression for V_n^s is difficult to obtain for any n [see in Equation (10)]; however, at the terminal ($n = 0$) it is given in (11b) leading to the requirement that $|\Gamma_0| \ll 1$. To this end, using Equation (11b) and noting that $|(\alpha - 1)/(\alpha + 1)| = \tan(\phi/2)$, this constraint suggests that

$$|\tilde{\delta}(\alpha)| \ll \left|\cot\left(\frac{\phi}{2}\right)\right| \tag{B1}$$

for all $\omega \in \Omega$. For $\xi \to 0$, i.e, $\phi \to 0$ ($\alpha \to 1$), it follows that $|\tilde{\delta}(\alpha)| \ll \infty$ which is redundant for any practical network. On the other hand, for $\xi \to (-4)$, i.e., $\phi \to \pi$ ($\alpha \to -1$), it follows that $\tilde{\delta}(\alpha)| \to 0$. Decomposing $\tilde{\delta}$ of Equation (11c) as $\tilde{\delta}(\alpha)|_{\alpha\to -1} = \sum_{m_e}(-1)^{-m_e}\bar{\delta}_{m_e} + \sum_{m_o}(-1)^{-m_o}\bar{\delta}_{m_o}$, where $m_{e,o}$ are even and odd $m = 0, 1, \ldots$ indexes, respectively, and recalling Equation (3c) that $\bar{\delta}_{m_o}$ and $\bar{\delta}_{m_e}$ are associated with $\bar{\delta}_{z_m}$ and $\bar{\delta}_{y_m}$, respectively, it follows that the perturbations should satisfy

$$\left|\sum_m \bar{\delta}_{z_m} - \sum_m \bar{\delta}_{y_m}\right| \to 0. \tag{B2}$$

Note that: (i) in the case where the actual span of the excitation frequencies is only a partition of Ω, the requirement in Equation (B2) should be lifted to a higher value, since $\min_\omega |\cot(\phi/2)| > 0$; and ($ii$) recalling the discussion preceding Equation (B1), if the backscattered voltage wave component of V_n^s is dominant over the forward scattered wave component, then $\Gamma_n = V_n^s/V_n^i$ can be approximated only by a backward component which upon requiring that $|\Gamma_n| \ll 1$, can yield an expression similar to Equation (B2), where the summation takes over forward indexes $n \le m \le N - 1$.

The condition stated in Equation (B2) can be satisfied in the following scenarios:

- *Each of the the two summations tends, separately, to zero* or if *the combined sum of the two perturbation sequences tends to zero.* This seems to suggest that the perturbations $\{\bar{\delta}_{z,y_m}\}$ can grow indefinitely as long as Equation (B2) is satisfied. However, one should recall that in obtaining Equation (11b) we have neglected second order perturbed terms in Equation (10). Therefore, $\{\bar{\delta}_{z,y_m}\}$ may grow as long as contributions due to second order or higher terms are negligible in comparison to first order contributions (this condition will be pursued elsewhere).

- Alternatively, since $|\tilde{\bar{\delta}}(\alpha)| \leq 2N \max_m\{|\bar{\delta}_m|\}$, it follows that $\max_m\{\bar{\delta}_{z,y_m}\} \ll |\cot(\phi/2)|/2N$, which pose much more restricted bounds on the weak scattering approximation than that taken in the previous item.

(ii) **Propagation type constraint:** The scattered voltage wave in Equations (9) and(11) was obtained by assuming that the actual network $\{\text{“}ZY_n\text{”}\}$ is “weakly” perturbed from the background network $\bar{Z}\bar{Y}$. Hence, assuming that wave propagation is dictated by the propagation constant of the background medium, $\alpha = e^{j\phi}$. However, the actual propagation is dictated by a different propagation constant, say, β, with $\beta = e^{j\phi_\beta}$. Noting that $\beta = \alpha e^{j(\phi_\beta - \phi)}$, it follows that some propagation *phase error* is accumulated along the propagation path. Therefore in order for the weak scattering approximation to hold, the phase error should be negligible ($\ll \pi$). To quantify this constraint, let us assume, for simplicity, that there are $M < N$ equally perturbed sections $\text{“}\bar{Z}_p\bar{Y}_p\text{”}$ with perturbations $\bar{\delta}_z$ and $\bar{\delta}_y$ and propagation constant satisfying $\beta^2 - (2+\xi_p)\beta - 1 = 0$, $\xi_p = \bar{Z}_p\bar{Y}_p$ (compare to Sec. 2.2). The propagation error along M sections is $M|\phi_\beta - \phi| \ll \pi$. Assuming weak scattering, expanding $\beta = \alpha + \Delta\alpha$ to first order in perturbation terms gives $\Delta\alpha \approx 2j\alpha\Delta\xi/\sin(\phi)$, and therefore, $\beta \approx \alpha(1+2j\Delta\xi/\sin(\phi))$ giving $\phi_\beta = \phi + \arctan(2\Delta\xi/\sin(\phi))$ with $\Delta\xi = \xi_p - \xi \approx \xi(\bar{\delta}_z + \bar{\delta}_y) = -4(\bar{\delta}_z - \bar{\delta}_y)/\sin^2(\phi/2)$. Thus, the phase error along one section is $|\phi_\beta - \phi| \approx |\arctan(4(\bar{\delta}_z - \bar{\delta}_y)\tan(\phi/2))|$. Consequently, along M sections the phase error is

$$\left|\arctan(4(\bar{\delta}_z - \bar{\delta}_y)\tan(\phi/2))\right| \ll \frac{\pi}{M}. \tag{B3}$$

The condition in Equation (B3) becomes most severe for $\phi \to \pi$ ($\alpha \to -1$). This condition is met whenever the two perturbation terms $\bar{\delta}_z, \bar{\delta}_y \to 0$ separately or $\bar{\delta}_z - \bar{\delta}_y \to 0$. Interestingly, if the perturbed part of the network is composed of many different perturbed subparts, each assembled from a number of uniform perturbed sections, the condition in Equation (B3) coincides with Equation (B2). It should be kept in mind that these conditions hold whenever higher order terms in Equation (10) are neglected.

REFERENCES

1. Ramo, J. S. and T. V. Duzer, *Fields and Waves in Communication Electronics,* 3rd Edition, John Wiley & Sons, Inc., 1994.
2. Collin, R. E., *Foundations for Microwave Engineering,* 2nd

edition, IEEE Press Series on Electromagnetic Wave Theory, IEEE Press, 2001.

3. Caloz, C. and T. Itho, *Electromagnetic Metamaterials, Transmission Line Theory and Microwave Applications,* IEEE Press, Hoboken, New Jersey, 2006.
4. Jaulent, M., "The inverse scattering problem for lcrg transmission lines," *J. Math. Phys.*, Vol. 23, No. 12, 2286–2290, 1982.
5. Zhang, Q., M. Sorine, and M. Admane, "Inverse scattering for soft fault diagnosis in electric transmission lines," *IEEE Transactions on Antennas and Propagation*, Vol. 59, 141–148, Jan. 2011.
6. Tang, H. and Q. Zhang, "An inverse scattering approach to soft fault diagnosis in lossy electric transmission lines," *IEEE Transactions on Antennas and Propagation*, Vol. 59, 3730–3737, Oct. 2011.
7. Bruckstein, A. M. and T. Kailath, "Inverse scattering for discrete transmissionline models," *SIAM Review*, Vol. 29, No. 3, 359–389, 1987.
8. Frolik, J. and A. Yagle, "Forward and inverse scattering for discrete layered lossy and absorbing media," *IEEE Transactions on Circuits and Systems II: Analog and Digital Signal Processing*, Vol. 44, 710–722, Sep. 1997.
9. Case, K. M. and M. Kac, "A discrete version of the inverse scattering problem," *J. Math. Phys.*, Vol. 14, No. 5, 594–603, 1973.
10. Berryman, J. G. and R. R. Greene, "Discrete inverse methods for elastic waves in layered media," *Geophysics*, Vol. 45, No. 2, 213–233, 1980.
11. Godin, Y. A. and B. Vainberg, "A simple method for solving the inverse scattering problem for the difference helmholtz equation," *Inverse Problems*, Vol. 24, No. 2, 025007, 2008.
12. Noda, S., "Wave propagation and reflection on the ladder-type circuit," *Electrical Engineering in Japan*, Vol. 130, No. 3, 9–18, 2000.
13. Ucak, C. and K. Yegin, "Understanding the behaviour of infinite ladder circuits," *European Journal of Physics*, Vol. 29, No. 6, 1201, 2008.
14. Parthasarathy, P. R. and S. Feldman, "On an inverse problem in cauer networks," *Inverse Problems*, Vol. 16, No. 1, 49, 2000.
15. Dana, S. and D. Patranabis, "Single shunt fault diagnosis in ladder structures 22 Shlivinski with a new series of numbers," *Circuits, Devices and Systems, IEE Proceedings G*, Vol. 138, 38–44, Feb. 1991.

16. Doshi, K., "Discrete inverse scattering," University of California, Santa Barbara, 2008.
17. Desoer, C. A. and E. S. Kuh, *Basic Circuit Theory,* McGraw-Hill, 1969.
18. Jirari, A., *Second-order Sturm-Liouville Difference Equations and Orthogonal Polynomials, Memoirs of the American Mathematical Society,* American Mathematical Society, 1995.
19. Felsen, L. B. and N. Marcuvitz, *Radiation and Scattering of Waves,* IEEE Press Series on Electromagnetic Waves, The Institute of Electrical and Electronics Engineers, New York, 1994.
20. Elaydi, S. N., *An Introduction to Difference Equations,* Springer-Verlag New York, Inc., Secaucus, NJ, USA, 1996.
21. Langenberg, K. J., "Linear scalar inverse scattering," *Scattering: Scattering and Inverse Scattering in Pure and Applied Science,* 121–141, Academic Press, London, 2002.
22. Tsihrintzis, G. and A. Devaney, "Higher-order (nonlinear) diffraction tomography: Reconstruction algorithms and computer simulation," *Processing of IEEE Transactions on Image*, Vol. 9, 1560–1572, Sep. 2000.
23. Tsihrintzis, G. and A. Devaney, "Higher order (nonlinear) diffraction tomography: Inversion of the Rytov series," *IEEE Transactions on Information Theory*, Vol. 46, 1748–1761, Aug. 2000.
24. Marks, D. L., "A family of approximations spanning the Born and Rytov scattering series," *Opt. Express*, Vol. 14, 8837–8848, Sep. 2006.
25. Markel, V. A., J. A. O'Sullivan, and J. C. Schotland, "Inverse problem in optical diffusion tomography. IV. Nonlinear inversion formulas," *J. Opt. Soc. Am. A*, Vol. 20, 903–912, May 2003.
26. Oppenheim, A. V., R. W. Schafer, and J. R. Buck, *Discrete-Time Signal Processing,* 2nd Edition, Prentice-Hall Signal Processing Series, Prentice Hall, 1999.
27. Devaney, A. J., "A filtered backpropagation algorithm for diffraction tomography," *Ultrasonic Imaging*, Vol. 4, No. 4, 336–350, 1982.